Adaptation of river channels to a wetter or drier climate
Insights from the Lower Pilcomayo River, South America

Crosato, A.; Grissetti-Vázquez, A.; Bregoli, F.; Franca, M.J.

DOI
10.1016/j.jhydrol.2022.128254

Publication date
2022

Document Version
Final published version

Published in
Journal of Hydrology

Journal of Hydrology 612 (2022) 128254

Contents lists available at ScienceDirect

Journal of Hydrology

journal homepage: www.elsevier.com/locate/jhydrol

Research papers

Adaptation of river channels to a wetter or drier climate: Insights from the Lower Pilcomayo River, South America

A. Crosato [a,b], A. Grissetti-Vázquez [a], F. Bregoli [c,*], M.J. Franca [a,b,d]

[a] IHE Delft Institute for Water Education, Delft, the Netherlands
[b] Faculty of Civil Engineering and Geosciences, Delft University of Technology, Delft, the Netherlands
[c] Department of Environmental Science, Radboud University, Nijmegen, the Netherlands
[d] Institute for Water and River Basin Management, Karlsruhe Institute for Technology, Karlsruhe, Germany

ARTICLE INFO

This manuscript was handled by Marco Borga, Editor-in-Chief, with the assistance of Francesco Comiti, Associate Editor

Keywords:
Alluvial river
Pilcomayo river
Climate change
Floodplain vegetation
River morphodynamics

ABSTRACT

Climate change has a direct influence on both hydrology and floodplain vegetation of water courses, which are key players in river morphodynamics. The river system response to climate change is complex and the effects of non-linear interactions between alterations in water, sediment and vegetation remain incompletely understood. Which of these components becomes dominant in shaping the river channel when climate becomes drier or wetter? To answer this question, we investigate the cross-sectional response of sand-bed rivers to climate change focusing on channel width and depth, which respond directly to changes in boundary stresses. Thanks to the exceptional availability of long time-series of daily discharge and cross-sectional profiles, the Pilcomayo River is an ideal living lab for this investigation. We constructed a two-dimensional model of the river using the open-source state-of-the-art, structured Delft3D code. The highly dynamic behaviour and quick morphological adaptation of the Pilcomayo allowed reducing the period of time covered by the simulations because the river cross-section adapts its morphology to a new value of the water discharge within hours or days, which is crucial for modelling investigations. Calibration and validation were successfully performed by comparison with historical data. We considered several scenarios representing current, dryer and wetter climates. The results show that a dryer climate reduces the river channel depth and enlarges the width. A wetter climate increases the channel depth but produces negligible widening. Vegetation, sparser with a drier climate and denser with a wetter climate, is found to control the channel width. This analysis is unique and shows which alterations can be expected in alluvial sand-bed rivers with natural vegetated banks due to climate change.

1. Introduction

Changing climate affects terrestrial landscapes (Baker, 1995; Yang et al., 2003) and their components through alterations in precipitation and temperature which directly affect water quantity and quality, soil erosion, soil moisture and vegetation cover (Masson-Delmotte et al., 2018; Seneviratne et al., 2006; Sperna Weiland et al., 2012; Trenberth, 2011). Increasingly frequent extreme events, such as floods and draughts, combined with deforestation, have already intensified sediment production and will govern the future geomorphological trends (Baker, 1995; Borrelli et al., 2017; Cai et al., 2014). Rivers have a primary role in transport and distribution of water, sediment and nutrients (Sabater et al., 2018; Wohl et al., 2015). Alterations in their discharge regime and sediment production (Church, 2006) induce changes in their morphology and dynamics, with consequences for the water conveyance and sediment transport (Grams and Schmidt, 2005; Kondolf, 1997; Wilby et al., 2008), as well as for the quality of their ecosystems (Wohl et al., 2015).

Floodplain vegetation plays a significant role on the morphological adaptation of rivers (Gurnell, 2014; Tal and Paola, 2010), since it affects the water flow distribution and sediment transport during floods (Lightbody et al., 2019; Villada Arroyave and Crosato, 2010; Wang et al., 2015), protects banks and emerging bars against erosion (Micheli and Kirchner, 2002; Rominger et al., 2010; Thorne, 1982), and creates the conditions for new floodplain formation (Hupp and Simon, 1991). As a result, dense vegetation growth on river banks and floodplains reduces the river braiding degree and promotes river meandering (Crosato and Saleh, 2011; Gibling and Davies, 2012; Gurnell, 2014, 2012; Nardi et al.,

* Corresponding author.
E-mail address: f.bregoli@science.ru.nl (F. Bregoli).

https://doi.org/10.1016/j.jhydrol.2022.128254
Received 15 February 2022; Received in revised form 15 June 2022; Accepted 21 July 2022
Available online 27 July 2022

2013; Solari et al., 2016; Tal and Paola, 2010; Ward et al., 2000). Isolated trees as well as sparse patchy vegetation, however, might split the flow promoting the excavation of channels through the floodplain and main channel bifurcation as well as enhancing local bank instability (Coulthard, 2005; Ielpi and Lapôtre, 2019; Vargas-Luna et al., 2019b). However, at the same time, floodplain vegetation growth also increases the water levels during floods (Villada Arroyave and Crosato, 2010).

By directly affecting the river discharge regime (Sperna Weiland et al., 2012), floodplain vegetation (Baker, 1995; Dale et al., 2001) and sediment production (Lane et al., 2007), climate change is thus expected to also modify the river morphology. This might have important consequences not only for the river landscape and ecosystem, but also for the river conveyance, the water accessibility, the safety of structures, the frequency of floods, and the human activities. This shows the relevance of anticipating and understanding river adaptation to climate change, which still remains a challenge (Harrison et al., 2019).

Reproducing the long term river response to climate changes in the laboratory, by combining the effects of altering discharge, sediment input and vegetation, requires a substantial effort. For this, if sufficient data are available, computational approaches represent a valid alternative (Arboleda et al., 2010; Siviglia and Crosato, 2016). Among the different types of water courses, sand-bed rivers show highly reactive responses to external drivers: they quickly adapt their alluvial channel to variations in discharge and sediment input through deposition, scouring, widening and narrowing (Martín-Vide et al., 2019; Sarker et al., 2014). Moreover, sand-bed rivers generally present full sediment mobility and their bed material can be assumed uniform (Singh et al., 2017). For this, simulating their morphological adaptation does not require excessively long computational times, which makes these systems ideal case studies to investigate the effects of changes in the main drivers of river morphology.

In the present research, we investigate how climate change affects the cross-section, and particularly the width and depth, of a natural sand-bed river using a two-dimensional numerical model of the Pilcomayo River at a location near the border between Paraguay and Argentina. We look at two of the main drivers of channel morphology which have a direct dependency on climate: river flow and floodplain vegetation. This study is made possible by the availability of a unique set of data, containing long time series of daily cross-sectional profiles and corresponding discharges. In addition, due to a bed composition of fine sand, the Pilcomayo River displays an extraordinary high dynamism (Martín-Vide et al., 2019), with fast adaptation to new environmental conditions, which allows estimating its morphological response to water flow and vegetation alterations with rather quick computations covering relatively short periods of time.

We consider moderate climate changes, corresponding to the 2100 projections of the Intergovernmental Panel on Climate Change (IPCC) Special Report on Emission Scenarios A1B, hereafter named as the SRES A1B scenarios (Stocker et al., 2013) based on which Sperna Weiland et al. (2012) derived the corresponding monthly changes in river discharge world-wide by running a multi-model ensemble of 12 general circulation models with the global hydrological model PCR-GLOBWB (Van Beek and Bierkens, 2009). For the Pilcomayo River, this scenario results in 20–30 % of flow reduction (Sperna Weiland et al., 2012). For sake of comparison, the scenarios analysed in this study are the present climate, the projected drier climate for the year 2100, as well as the opposite wetter climate. Each scenario is represented by a water discharge regime, derived from the work of Sperna Weiland et al. (2012), affecting also the input/output of sediment in the study area, and floodplain vegetation. The three adopted discharge scenarios represent well the range of variability that more recent global change scenarios displayed. For instance, Montroull et al. (2018) analysed the impact of adopting several representative concentration pathways, RCPs (van Vuuren et al., 2011), on future streamflow scenarios in la Plata basin where the Pilcomayo lays. Their conclusion is that the percentage of change in annual mean streamflow in the basin is between −20 % to + 25 %. These values are in line to our dry and wet scenarios.

There are no quantitative studies on how on-going global warming will change vegetation, but observations show that richer vegetation is found in wetter climates and sparser vegetation in drier climates (Anadón et al., 2014; van Oorschot et al., 2018). The vegetation scenarios considered in this study are based on these observations, which means that floodplain vegetation is assumed to be higher and denser with the considered wetter climate; sparser and shorter with the drier climate.

2. The Pilcomayo river

The Pilcomayo River flows south-eastwards from the Andes to the Paraguay River, a tributary of the Paraná, for 1,100 km. Its basin is part of the La Plata Basin, the second largest one in South America after the Amazon (Martín-Vide et al., 2014). The study area is an 8 km long river reach of the Lower Pilcomayo near the border between Paraguay and Argentina. This zone includes the gauging station Misión La Paz (Argentina) where the river has a catchment area of 96,000 km^2. At this location, the Pilcomayo divides the Argentinian village of Misión La Paz from the Paraguayan village of Pozo Hondo, whereas a 220-metre-long international bridge connects the two communities. The study reach starts 4 km upstream and ends 4 km downstream of this bridge. The river has a meandering style and no tributaries (Fig. 1). It has a mild slope (about 0.03 %), an average main channel width varying from 75 m to some hundreds meters as a function of discharge, and wide floodplains covered by sparse vegetation, mainly consisting of semi-open shrub. At low-flow conditions, the river bed presents many sand bars and areas of lateral sediment deposition (Fig. 1).

The river bed material is fine sand, with particles ranging between 0.1 and 0.2 mm, as indicated by Pool and van Duijne (1996). The yearly sediment transport rate of this reach of the Pilcomayo River is estimated in 140 million tons/year, for 89 % composed of silt and clay (wash load not contributing to the morphological changes of the river channel in the study area and thus not considered in this study), and for 11 % of fine sand (Martín-Vide et al., 2014).

According to the updated Köppen-Geiger classification (Peel et al., 2007), the climate of the Pilcomayo basin is temperate, with total yearly precipitation ranging between 400 and 500 mm (upper basin) and 700–1,200 mm (lower basin) and yearly averaged temperatures of 9.5 °C and 23.3 °C, respectively (Halcrow & Serman Associados, 2006). As far as 90 % of the annual precipitation occurs in the period mid-November to mid-March. Concentration of rainfall in such a short time causes two physical processes, outstanding in the entire basin: large floods and intense fluvial erosion/deposition (Pool and Van Duijne, 1996). An important part of the river catchment lies inside the Gran Chaco, a hot semi-arid lowland region between the Andes and the Paraguay River with poor vegetation cover and high soil erodibility.

The National Hydrological Network of Argentina has records of daily discharges, water levels at the station of Misión La Paz covering the periods November 1960 to August 2018 and September 1964 to July 2019, respectively. At this location, the maximum recorded discharge is 4,585 m^3/s (in March 1984) and the minimum is 1.4 m^3/s (in October 1972), the mean annual discharge being 212 m^3/s. The wet season is from December to March. The maximum value of monthly discharge is 648 m^3/s and it corresponds to February, while the month with less discharge is September, with an average discharge of 22 m^3/s.

The strong flow variability, combined with a highly erodible bed composed of fine sand and sparse riparian vegetation, makes the Lower Pilcomayo a notoriously dynamic river with cross-sections responding very fast to flow variations (Capape and Martin-Vide, 2015; Martín-Vide et al., 2014; Pool and Van Duijne, 1996). This can be observed in the video provided by Martín-Vide et al. (2019) as supplementary material (https://ars.els-cdn.com/content/image/1-s2.0-S0022169419305888-mmc1.mp4, retrieved the 1st December 2020). This is clear also when analysing the daily cross-sectional data collected by the Tri-National

Fig. 1. The Pilcomayo River: upper left panel, the study area location within South America; upper right panel, map of the region with the Pilcomayo Basin in gray shade; main figure: an aerial photography of the river close to Misión La Paz looking downstream, taken in June 2017 (courtesy of Kenny Goossen).

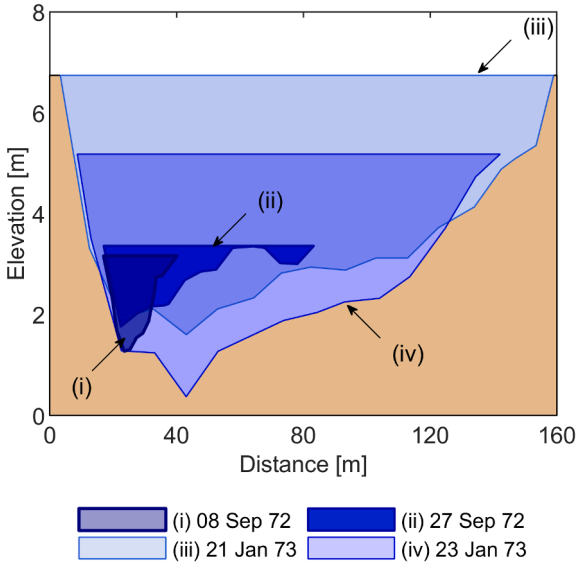

Fig. 2. Channel cross-section A, looking in the downstream direction, at Misión La Paz measured in the period 1972–1973 showing strong and quick morphological variations in time. The corresponding discharges are: (i) 12 m^3/s; (ii) 25 m^3/s; (iii) 1,330 m^3/s; and (iv) 550 m^3/s. Discharge and cross section geometries data were obtained from the Tri-national Committee for the Development of the Pilcomayo River basin (www.pilcomayo.net). Their measuring technique is well described in Martín-Vide et al. (2019).

Committee for the Development of the Pilcomayo River basin at the two locations near Misión La Paz in the period 1972–2019 (Fig. 2). As consequence of bank erosion rates, also the channel alignment continuously changes (Fig. 3). The current reach-scale characteristics of the Pilcomayo River in the study area are summarized in Table 1.

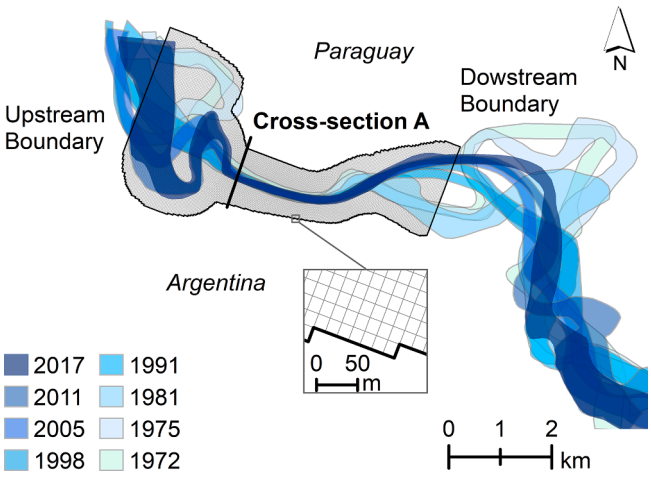

Fig. 3. Changes of river course in 45 years (1972–2017), as manually derived from selected Landsat images (see section 3.2 for further details on used Landsat images). The Cross-Section A (black line) is located at the gauging station of Misión La Paz (22°22′38″S, 62°31′24″W). The black polygon represents the numerical model domain, which contains the river channels in the period 1972–2019 for an extension of 8 km. The rectangular grid cells are shown in the small square.

Table 1
Current reach-scale characteristics of the Pilcomayo River at Misión La Paz: average values in bold and range of values in brackets if available.

Discharge [a] (m^3/s)	Channel width [b] (m)	Longitudinal slope [c] (%)	Sinuosity [c] (-)	Bed grain size [d] (mm)
212 (1.4 – 4,585)	(75 – 180)	**0.038**	**1.30**	(0.10 – 0.20)

[a] - Measured values in the period 1960–2018;
[b] - measured at Cross-Section A in the period 1972–2019 by the Tri-National Committee for the Development of the Pilcomayo River basin;
[c] - average of the period 1972–2017;
[d] - data from Kopaliani and Georgievsky (1993) with no information regarding temporal variations.

3. Materials and methods

The analysis of daily data series, covering long periods of time, allows properly setting up, calibrating and validating a reliable numerical model simulating the morphological behaviour of the Pilcomayo River. The type of sediment forming the alluvial bed (fine sand) allows assuming full sediment mobility and thus considering a single sediment size in the model, reducing computational time (Singh et al., 2017). Moreover, due to the extremely quick response of the river to changing conditions, simulating a single hydrological year can be considered enough to detect the range of effects of alterations in morphological drivers. All these factors together make the Pilcomayo a unique case to be used as a living lab to investigate the response of alluvial sand-bed rivers to climate change.

3.1. Model description

We constructed a two-dimensional (2D) numerical model of the Pilcomayo River using the open-source structured Delft3D code (version 4.1), which solves the 3D Reynolds equations for shallow water coupled to sediment transport and sediment balance equations, including also a bank erosion formulation (Deltares, 2019; Lesser et al., 2004), downloadable at https://oss.deltares.nl/web/delft3d. The code has been widely tested and validated for investigations requiring the simulation of the morphological changes of rivers with vegetated floodplains (e.g.: Arboleda et al., 2010; Vargas-Luna et al., 2018; Villada Arroyave and Crosato, 2010). The model computes water levels and depth-averaged flow velocity, the latter as a vector with two components in the horizontal plane, as well as changes of bed topography and channel alignment, including the effects of vegetation on local energy dissipation and sediment transport rate. Bed level changes are computed at every time step for every grid cell based on sediment budget, following Exner (1920) approach, in which the sediment transport rates are computed using a sediment transport capacity formula:

$$(1-\varepsilon)\frac{\partial z_b}{\partial t}+\frac{\partial S_x}{\partial x}+\frac{\partial S_y}{\partial y}=0 \tag{1}$$

where, ε is the bed porosity, z_b is the bed level, t is time, S_x is the sediment transport rate in the x-direction and S_y is the sediment transport rate in the y-direction.

In river bends, the stream lines have a spiral shape with important vertical flow components near the banks. The maximum flow velocity is shifted towards the outer bend, altering the bed shear stress direction. This affects the sediment transport direction, with relevant consequences for the computation of channel bed topography (Struiksma et al., 1985). Another factor influencing the sediment transport direction is gravity, which is particularly relevant for bed load if the bed is sloping. The presence of bars and pools produces important transverse slopes, which should be considered by the model. The sediment transport direction is therefore corrected by taking into account both the spiral flow and the gravity effects, following Koch and Flokstra's (1980) formulation:

$$\tan\alpha_S=\frac{\sin\alpha_T-\frac{1}{f}\frac{\partial z_b}{\partial y}}{\cos\alpha_T-\frac{1}{f}\frac{\partial z_b}{\partial x}} \tag{2}$$

where α_S is the direction of sediment transport and α_T is the direction of bed shear stress. f is a user-defined tuning parameter, which we computed according to Talmon et al. (1995):

$$f=A_{shld}\theta^{Bshld}\left(\frac{D_{50}}{h}\right)^{Cshld} \tag{3}$$

where θ is the Shields parameter, D_{50} is the median sediment grain size, h is the local water depth and A_{shld}, B_{shld} and C_{shld} are calibration coefficients.

The model represents bank erosion by transferring a fraction of the erosion occurring at every wet cell to the adjacent dry cell (if present), which then becomes wet and is then incorporated in the water flow and morphological computations (van Der Wegen and Roelvink, 2008). For the Pilcomayo River, 80 % of the erosion computed for a cell at the bank toe is transferred to the adjacent floodplain cell, with the result of enlarging the wet channel width.

The effects of vegetation on water flow and sediment transport are taken into account by adjusting the flow resistance as a function of vegetation characteristics. Two roughness coefficients are computed: the global Chézy coefficient, for the derivation of the depth-averaged hydraulic variables, and a Chézy coefficient of the soil among the plants, for the derivation of the bed shear stress and the sediment transport rate, following Baptist's formulation (Baptist et al., 2007). The method distinguishes between submerged and emerging vegetation. Plants are represented as vertical rigid cylinders (Vargas-Luna et al., 2016) with specific density, height and diameter. The flow velocity is considered uniform through the plants but following a logarithmic vertical profile above the canopy. The total shear stress is assumed to be composed of two components:

$$\rho ghi=\tau_b+\tau_v \tag{4}$$

in which ρ is the water density, g is the acceleration due to gravity, h is the local water depth, i is the longitudinal water surface slope, τ_b is the bed shear stress and τ_v is the extra shear stress caused by the presence of vegetation.

For emerging plants, the water depth h is smaller than the plant height, h_v. In this case, the two stresses can be written as:

$$\tau_b=\frac{\rho g}{C_b^2}u_v^2 \tag{5}$$

$$\tau_v=\frac{1}{2}\rho C_D m D h u_v^2 \tag{6}$$

where C_b is the Chézy coefficient of the un-vegetated bed, u_v is the flow velocity through vegetation, C_D is the drag coefficient of the plants, m is the vegetation density per unit area and D is the representative stem diameter, the product mD being the canopy density, a, defined by Nepf (2012). The global Chézy coefficient, C_r, is obtained by combining the two equations with the Chézy equation$u_v = C_r\sqrt{hi}$, leading to:

$$C_r = \sqrt{\frac{1}{\frac{1}{C_b^2} + \frac{C_D m D h}{2g}}} \quad (emerging\ vegetation) \tag{7}$$

If the plant height is smaller than the local water depth (submerged vegetation), the flow is assumed to be split in two parts: the flow through the plants and the flow above the canopy. In this case:

$$C_r = \sqrt{\frac{1}{\frac{1}{C_b^2} + \frac{C_D m D h_v}{2g}}} + \frac{\sqrt{g}}{\kappa} ln\left(\frac{h}{h_v}\right) \quad (submerged\ vegetation) \tag{8}$$

in which κ is the van Kármán constant ($\kappa = 0.41$) and h_v is the plant height. The bed shear stress, τ_b, is computed as:

$$\tau_b = \frac{\rho g}{C_b^{2'}} \overline{u}^2 \tag{9}$$

where $\overline{u}$ is the depth-averaged flow velocity for which $\overline{u} = C_r\sqrt{hi}$ and $C_b^{'}$ is the Chézy coefficient of the soil among the plants, which is used to compute the bed shear stress and the sediment transport rate in the vegetated areas. Its value is a function of C_b, the Chézy coefficient of the un-vegetated bed, corrected to take into account the effects of vegetation, which is obtained as:

$$C_b^{'} = C_b + \frac{\sqrt{g}}{\kappa} ln\left(\frac{h}{h_v}\right)\sqrt{1 + \frac{C_D m D h_v}{2g}} \tag{10}$$

For emerging vegetation:$C_b^{'} = C_b$.

3.2. Model set up

Considering the significant planimetric changes that occurred in the study area, three distinct numerical models were constructed to represent the Pilcomayo River in three different periods of time for which long and complete daily data series are available: 1972/1973; 1980/1981 and 2017/2018. The historical river models 1972/1973 and 1980–1981 were meant for calibration and validation purposes. The model of the river in 2017–2018 was used as the morphological starting point for the study of the climate scenarios. The following satellites images were used to reconstruct the historical river-bank alignments:

- Periods 1971/1972 and 1980/1981: Landsat 1–3, Level-1 (retrieved from United Station Geological Survey at https://earthexplorer.usgs.gov).
- Period 2017/2019: Landsat 8, Level-1 (retrieved from United Station Geological Survey at https://earthexplorer.usgs.gov).

In the study reach, the bankfull river width between 100 m to several hundreds of meters. Landsat 1–3, Level-1 images have a resolution of 60 m. Therefore, a minimum of 1 full pixel (or 1.67 pixels) to a maximum of about ten full pixels fit the river width. This is enough to recognize and depict the main river channel bankfull width. Landsat 8, Level-1 images have a resolution of 30 m. Therefore, the river width is depicted with a minimum of 3 full pixels (or 3.33 pixels). The river banks were manually depicted. The resulting historical river planimetries are shown in Fig. 3.

Topographical elevations were derived using the ALOS (Advanced Land Observing Satellite) DEM of 2011, with resolution of 12.5 × 12.5 m^2, covering an area of 30 km^2 (downloaded from: https://www.asf.alaska.edu/sar-data/palsar/terrain-corrected-rtc/). Irregularities in the DEM were smoothed out using ArcGIS's geoprocessing tools, process that was finalized using the QUICKIN tools of the Delft3D software package.

The spatial distribution of floodplain vegetation was obtained from the Google Earth images 1984 to 2016 in a straightforward way, by defining the contourlines of the areas presenting the same vegetation cover. The current plant characteristics were derived from local photos and simple field observations, indicating that floodplain vegetation in the study area can be classified as semi-open shrub constituted by 3 m high plants with a density of approximately 7 stems/m^2. Data on growth rates, conditions for germination, establishment and decay, as well as root characteristics of floodplain vegetation are missing. This lack of data makes impossible to model the interaction between plant dynamics (variations in vegetation characteristics due to colonization, growth and decay of plants) and the morpho-dynamics of the Pilcomayo River (O'Hare et al., 2016; Pasquale et al., 2014; Perona et al., 2012). Caponi et al. (2020) indicate that vegetation does not establish on migrating bars in case of high uprooting rates during floods. The Pilcomayo presents powerful and relatively frequent flood events, with bars that appear and disappear very quickly. This extremely high morphodynamics results in regular removal of sprouts from bars, point bars and channel margins. Fig. 1 shows the almost complete absence of vegetation growth on these areas. Instead, vegetation is present on the river floodplains, where is appears as a rather uniform semi-open shrub. It is therefore appropriate to suppose that plant dynamics does not influence the current morphological developments of the Pilcomayo River channel in a significant way (Boothroyd et al., 2021).

The model domain was discretized in more than 27,000 cells with dimension between 12 × 15 and 30 × 30 m (Fig. 3). The upstream boundary conditions consist of water and sediment inflows. Water inflow is made up of a daily discharge time. The sediment inflow is computed as local sediment transport capacity, derived as a function of flow velocity, particle size, bed roughness and other parameters adopting the best performing sediment transport formula (van Rijn, 1984). Due to the absence of measured water levels time series at a location close to the end of the model domain, the downstream boundary conditions are water levels and sediment outflows being calculated by the model assuming uniform flow. The initial bed topography of each historical model was derived numerically. It was obtained by running the model for the last 18 months before starting the scenario runs using the measured daily discharges (spin up runs). Before this, a preliminary channel was created by lowering the levels in the area between the river banks by 2.5 m.

Summarising, the three historical model setups have different initial river bank alignment and bed topography, floodplain vegetation cover distribution, and different upstream and downstream boundary conditions, but the same numerical grid, sediment transport formula and physical parameters, either derived from the calibration procedure or from physical considerations.

3.3. Model calibration and validation

Model calibration was carried out by optimizing the values of several coefficients to best reproduce the river morphological behaviour in the period 1972/1973 imposing initial morphological conditions corresponding to the river alignment of 1972 and model-generated 2D bed topography. The upstream boundary conditions of this model were the series of daily discharges measured in the same period. The sediment input rate was computed as a function of incoming discharge. The chosen calibration period can be regarded as a typical hydrological year of the Pilcomayo River, with a maximum discharge of 1,362 m^3/s and an average discharge of 173 m^3/s.

Vegetation, described by plant height, representative stem diameter and density was assumed to be equal to the current climatic condition (Section 3.4), but with the 1984 spatial distribution, derived from Google Earth (lack of historical information on floodplain vegetation prevented us to define the vegetation distribution before 1984).

In the calibration process, special attention was paid to obtain a good characterisation of the river dynamics, represented by the temporal variations of maximum water depth, measured at the deepest point (thalweg) in the monitored cross-section. The River Pilcomayo does not have a dominant horizontal bed structure on which to calibrate a 2D model, because its bed topography changes with high speed every day, showing daily appearance and disappearance of bars and shoals, as a response to discharge variations (Fig. 2 and Fig. 3). It was therefore

meaningful to calibrate the model in such a way that it captures the measured river dynamics. Compared to the cross-section averaged bed level, the thalweg level incorporates some information on cross-sectional shape. For instance, the average bed level hardly responds to the formation of bars. The presence of alternate bars would deepen the thalweg without changing the average bed level significantly. Moreover, the thalweg would be deeper with alternate bars rather than with central or multiple bars (Crosato and Mosselman, 2009).

Besides the temporal variation of the maximum water depth, calibration was based also on the temporal variations of the wet cross-sectional area, and on the yearly volume of transported sediment on the basis of the best performance compared to measured data. To decide which calibration simulation is the best performing one, a multi-criteria analysis was carried out by computing the coefficient of determination (R^2), the root mean square error (RMSE), and the mean absolute error (MAE), relative to wet area and maximum water depth of the cross-section, for each specific calibration run by comparing computed and measured values (Moriasi et al., 2015). The calibration parameters are the following:

- Chezy's coefficient of bare bed: the same value for main channel and floodplain soil, corresponding to C_b in Equations 4–10.
- Chezy's coefficient of the vegetated floodplains: the Baptist's method allows deriving two values of Chezy's coefficient from the bare-bed roughness coefficient, C_b, and the plant characteristics, one to be used for the computation of the hydrodynamic characteristics (either Equation 7 or 8) and the other one for the bed shear stress (Equation (10)).
- Transverse slope effects on the sediment transport direction, where A_{shld}, α_S and α_T are calibration parameters (Equations (2) and (3)).
- Multiplication factor for suspended sediment concentration formula of van Rijn (1984).
- Multiplication factor for bed-load transport vector magnitude of the formula of Engelund and Hansen (1967).

The downstream boundary conditions affect not only the flow distribution and the morphological changes in the last part of the model domain but might gradually impact also the areas more upstream if undesirable backwater effects are created. For this reason, due to the absence of water level measurements close to the model boundary, the calibration process included also the selection of the best-performing downstream boundary condition.

Model validation was carried out to assess the model performance based on an independent set of data, i.e. on the morphological changes that occurred in the period 1st January 1980 to 28th February 1981 starting from the 1980 channel alignment and model-generated bed topography. The model was run using the daily discharges measured in the same period with the values of calibration coefficients derived from the calibration procedure and with the spatial distribution of vegetation of 1984 and plant characteristics of current climate described in Section 3.4.

3.4. Climate scenarios

Sperna Weiland et al. (2012) estimated a 25 % discharge reduction in December, January and February (wet season), a 30 % reduction in March to August, and a 20 % reduction in September to November (dry season) in the study area. To have a mirror condition for comparing purposes, we consider also a wetter climate (Wet), presenting the same percentages of discharge variations of the projected scenario, but in opposite direction. This means that we consider three different hydrographs (Fig. 4):

1) the one representing the current situation (Base-Case), Q BC, corresponding to the series of discharges measured in the period September 2017 to August 2018;

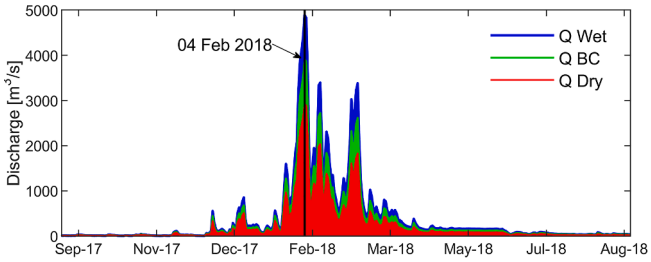

Fig. 4. The three discharge hydrographs considered in the model, constructed from the measured discharges in the period September 2017 to August 2018, which can be regarded as a typical hydrological year. Legend: green = present climate; blue = higher discharges (wetter climate); red = lower discharges (drier climate). Legend: Q Wet = discharge hydrograph of the wet climate scenarios; Q BC = present discharge hydrograph (Base current scenarios); Q Dry = discharge hydrograph of the dry climate scenarios (based on SRES A1B IPCC projections). (For interpretation of the references to colour in this figure legend, the reader is referred to the web version of this article.)

2) a constructed dryer hydrograph, Q Dry;
3) a constructed wetter hydrograph, Q Wet.

The current total yearly runoff is 9,935 Mm^3, the one relative to the constructed wet hydrograph is 12,598 Mm^3 (+26.8 %), whereas for the constructed dry hydrograph, the total yearly runoff is 7,272 Mm^3 (–26.8 %).

Due to expected differences in soil moisture, the drier climate is assumed to also present reduced floodplain vegetation mass (Anadón et al., 2014; Stocker et al., 2013); the wetter climate increased vegetation mass (van Oorschot et al., 2018). More specifically, considering that the current floodplain vegetation in the area is a semi-open shrub, we assume that this would turn into open shrub for the climate becoming drier and into close shrub for the climate becoming wetter. In total, we consider four vegetation scenarios, since we also include a case without floodplain vegetation. The present distribution of floodplain vegetation is used for all scenarios. According to observations and to Baptist and de Jong (2005), we introduce the following plant heights and canopy densities in the model: for the semi-open shrub, 3 m high plants with a canopy density of 0.07 m^{-1}, corresponding to the current plant characteristics; for the open shrub, 2.5 m high plants with a canopy density of 0.034 m^{-1}; for the close shrub, 3.5 m high plants and canopy density of 0.102 m^{-1}. All plants have a representative stem diameter of 0.01 m. Finally, we assume the drag coefficient of the plants to be $C_D = 1$, as suggested by Vargas-Luna et al. (2016). Regarding vegetation dynamics, in terms of vegetation colonization, growth and decay, it is supposed that these processes do not affect the morphological developments of the Pilcomayo River in a significant way also for the moderately drier and wetter climates. In drier climates vegetation grows slower and is less dense. This diminishes the mutual protection offered by plants, enhancing bed erosion around plants and eradication, partly counterbalancing the flow reduction (although in drier climates the flood intensity might increase, see discussion). In wetter climates vegetation grows faster and denser, but at the same time the water flow increases, partly counterbalancing the increase in plant resistance. Note that this is only valid for moderate climate changes.

The bare soil of the floodplains among the plants is assumed to have the same roughness as the main channel bed for which we assign the calibrated value of Chézy coefficient: $C_b = 60$ $m^{1/2}/s$. This is used to compute the hydraulic variables and bed shear stress for the case without vegetation. It is also used to compute the bed shear stress if plants are emerging, but if vegetation is submerged the model computes the bed shear stress using C_b' (Equation (10)). Note that for vegetated areas the hydraulic variables, such as the depth-averaged flow velocity and the water depth, are computed using the global Chézy coefficient, C_r (Eqs. (7) and (8)). The spatial distribution of vegetation is assumed equal

Table 2
Description of the scenarios.

Scenario	Description	Total cumulative runoff (Mm^3)	Plant height (m)	Canopy density (m^{-1})
BC Veg	Current discharge, current vegetation: semi-open shrub	9,935	3.0	0.070
Current Climate				
BC Veg(-)	Current discharge, reduced vegetation: open shrub	9,935	2.5	0.034
BC Veg(+)	Current discharge, increased vegetation: close shrub	9,935	3.5	0.102
BC noVeg	Current discharge, without vegetation	9,935	0	0
Dry Veg	Reduced discharge, current vegetation: semi-open shrub	7,272	3.0	0.070
Dry Veg(-)	Reduced discharge, reduced vegetation: open shrub	7,272	2.5	0.034
Drier Climate				
Wet Veg	Increased discharge, current vegetation: semi-open shrub	12,598	3.0	0.070
Wet Veg(+)	Increased discharge, increased vegetation: close shrub	12,598	3.5	0.102
Wetter Climate				

to the present one, derived from Google Earth. For all climatic scenarios, the sediment input rates coincide with the transport capacity of the incoming flow, computed using van Rijn's (1984) formula, and depend thus on discharge regime. This approach neglects wash load, i.e. the sediment transported in suspension with size of the order of several micrometres (clay and silt). This sediment does not affect the morphology of dynamic rivers and can thus be neglected from this study, focusing on river channel adaptation.

In total, we simulated eight scenarios, combining the three discharge hydrographs (current, wetter and drier) with the three different classes of vegetation, plus one case without vegetation (Table 2).

The analysis of combinations of these scenarios allows isolating the effects of discharge, vegetation and climate. All scenario runs started from channel alignment and model-generated bed topography of the year 2017.

4. Results of model calibration and validation

The best performing set of input parameters was identified based on 49 runs, each one differing in the value of one or more calibration coefficients or parameters which were always falling within their physics-sound range. As an example, the range of values of Chézy's coefficient considered in the calibration runs was derived from the results of previous hydrodynamic computations performed using Manning's coefficient (Baldissone et al., 2013; Brea et al., 2014; Testa Tacchino, 2015) concluding that the values to be used for the Pilcomayo River in the study area fall between 0.018 $s/m^{1/3}$ and 0.020 $s/m^{1/3}$, which correspond to Chézy's coefficients in the range of 50 to 65 $m^{1/2}/s$, with the highest values for high flow conditions. The sediment particle diameter was optimized by considering only values falling within the measured range to comply with the estimated value of total yearly sediment transport (Fernández and Garcia, 2017). The calibration phase also included the selection of the sediment transport formula. Note that the sediment transport formula affects not only the sediment transport rates in the study area, but also the sediment inputs from upstream and the speed of the morphological developments. About the correction of sediment transport direction due to spiral flow and gravity (Eq. (3)), we calibrated the coefficient A_{shld}, being the one that mostly affects the river bed topography, whereas the other two coefficients were given their default values: $B_{shld} = 0.5$ and $C_{shld} = 0.3$. The time step used in the computations was nine seconds, selected based on preliminary runs.

The results of the calibration runs show that the best performing downstream boundary condition is the water level recomputed at each time step assuming uniform flow with a value of Chézy's coefficient equal to 60 $m^{1/2}/s$. This is the calibrated value of the roughness coefficient for the un-vegetated river bed and floodplains composed of sediment having diameter equal to 0.1 mm. The best-performing value of the coefficient weighing the effects of gravity on sediment transport direction, A_{shld}, is 0.5, corresponding to a relatively high sediment transport deviation towards the deepest areas of the river bed (Baar et al., 2019). The best-performing sediment transport formula is the one developed by van Rijn (1984), which is particularly suited for sand-bed

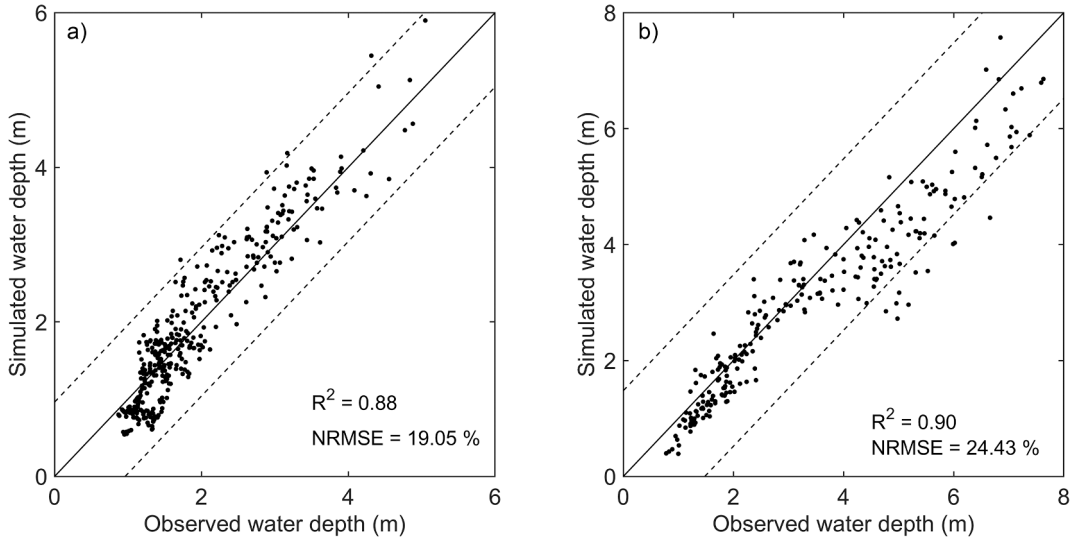

Fig. 5. Results of model calibration and validation for Cross-Section A (Fig. 3). a) Model calibration: observed vs simulated maximum water depth - September 1972 to September 1973 (maximum discharge 1,362 m^3/s). b) Model validation: observed vs simulated maximum water depth - January 1980 to February 1981 (maximum discharge 1,868 m^3/s). 1:1 relationship in solid line; dashed lines represent the range of the deviation by 1.5 times the average measured water depth in the respective periods of calibration and validation. The NRMSE is calculated as the RMSE normalized by the average measured water depth.

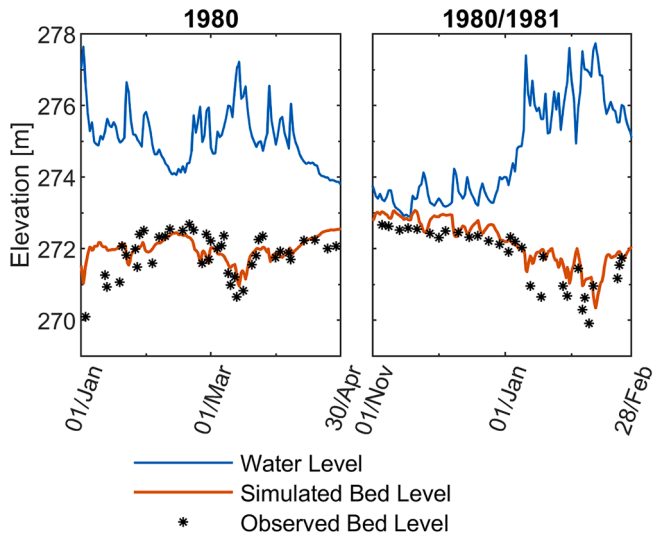

Fig. 6. Results of model validation: simulated thalweg levels (brown lines) and water level (blue lines) and measured thalweg levels (black stars) at Cross-Section A (Fig. 3) for two different periods in 1980 and 1981 (maximum discharges 1,817 m^3/s and 1,868 m^3/s, respectively). (For interpretation of the references to colour in this figure legend, the reader is referred to the web version of this article.)

rivers and distinguishes bed load from suspended load.

Fig. 5a illustrates the results of model calibration with remarkable values of R^2 and normalized root mean square error (NRMSE) for the maximum water depth in Cross-Section A (location indicated in Fig. 3). Particularly, after calibration, the error is limited to 19 %. The MAE relative to maximum water depth resulted in 0.31 m and the MAE relative to cross-sectional wet area in 31.34 m^2.

The results of the validation run are shown in Fig. 5b and Fig. 6. Fig. 5b illustrates the simulated water depth versus its corresponding measured values, showing values of R^2 and normalized root mean square error (NRMSE) being similar to the ones of the calibration period. Additionally, Fig. 6 depicts the comparison between measured and computed bed levels showing a high-quality performance of the model. The simulated bed levels follow well the pattern of observed data, indicating that the model can successfully reproduce the observed cross-sectional morphological adaptation of the river.

5. Results of scenario runs

5.1. Effects of discharge and vegetation on main channel cross-section

Fig. 7 shows the cross-sectional profiles at high flow conditions (February 4th 2018, Fig. 4). In this case, the main channel width coincides with the river bankfull width (e.g.: Vargas-Luna et al., 2019a; Wilkerson and Parker, 2011). For smaller discharges the model would give the width and the depth of the water flowing within the main channel, which would not represent the channel size, but just the lateral and vertical dimensions of the wet area at that particular flow rate. Moreover, at flows smaller than or equal to the bankfull discharge, the water would not flow through the side channels, making them hard to be recognized/visualized from the model results.

Fig. 7a indicates the effects of floodplain vegetation, since it presents the results of four runs with the same water and sediment inputs (hydrograph Q BC, corresponding to the Base Case flow) and different floodplain vegetation characteristics. The cross-sectional profiles show that higher vegetation mass (Veg (+): thin green line) enhances levee formation and concentrates the water flow in the main river channel. As a result, the channel becomes deeper, complying with the observations of Gurnell (2014). Lower vegetation mass (Veg(-): dotted green line) results in more distributed sediment deposition over the floodplains and in a shallower channel. In this scenario, the channel of the Pilcomayo presents a shift of a few tens of meters toward the right bank of the river due to enhanced bank erosion and sediment deposition near the opposite bank. Finally, the extreme scenario in which vegetation is absent results in a relevant main channel shift to the left and in the formation of a small secondary channel to the right (noVeg: black dotted line). The main channel is wider and shallower, and presents a central bar. This is due to morphodynamic instability triggered by the high width-to-depth ratio of the flow (e.g.: Crosato and Mosselman, 2020). The irregular cross-section is a clear indication of channel braiding (Leopold and Wolman, 1957).

Fig. 7b shows the effects of having a different discharge regime. The results of the scenarios with the current floodplain vegetation characteristics (Veg), indicate that higher discharges (Wet: dotted blue line) produce a deeper channel contained by larger levees. Smaller discharges (Dry: dotted red line) produce a shallower channel and smaller levees. Due to the presence of vegetation on banks and floodplains, the width of the channel appears to be only slightly influenced by the discharge regime. However, this conclusion is only valid for moderate changes in water flow, as in the studied scenarios, with well-developed floodplain vegetation, as in the study area. The smaller discharge regime does not alter the channel width, whereas the channel presents some widening with the largest one. This is due to the higher near-bank flow velocities that are capable of eroding banks despite the presence of vegetation.

5.2. Effects of climate change on channel cross-section and river fluvial style

Fig. 8 shows the Cross-Section A profiles that are obtained for the three considered climate scenarios on different days. The extremely fast

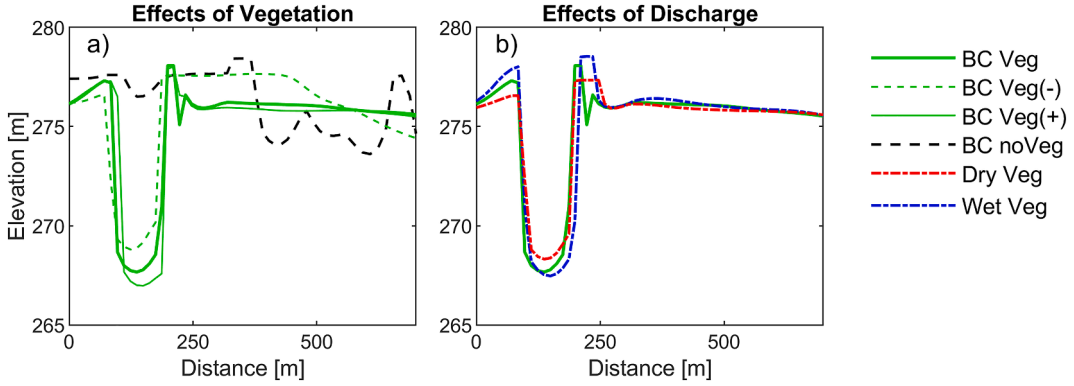

Fig. 7. Simulated Cross-Section A profiles (Fig. 3) on 04 Feb 2018 (Fig. 4) seen from downstream. The horizontal axis represents the distance from the right bank. a) Four vegetation scenarios and current hydrograph. b) Three discharge scenarios and current floodplain vegetation.

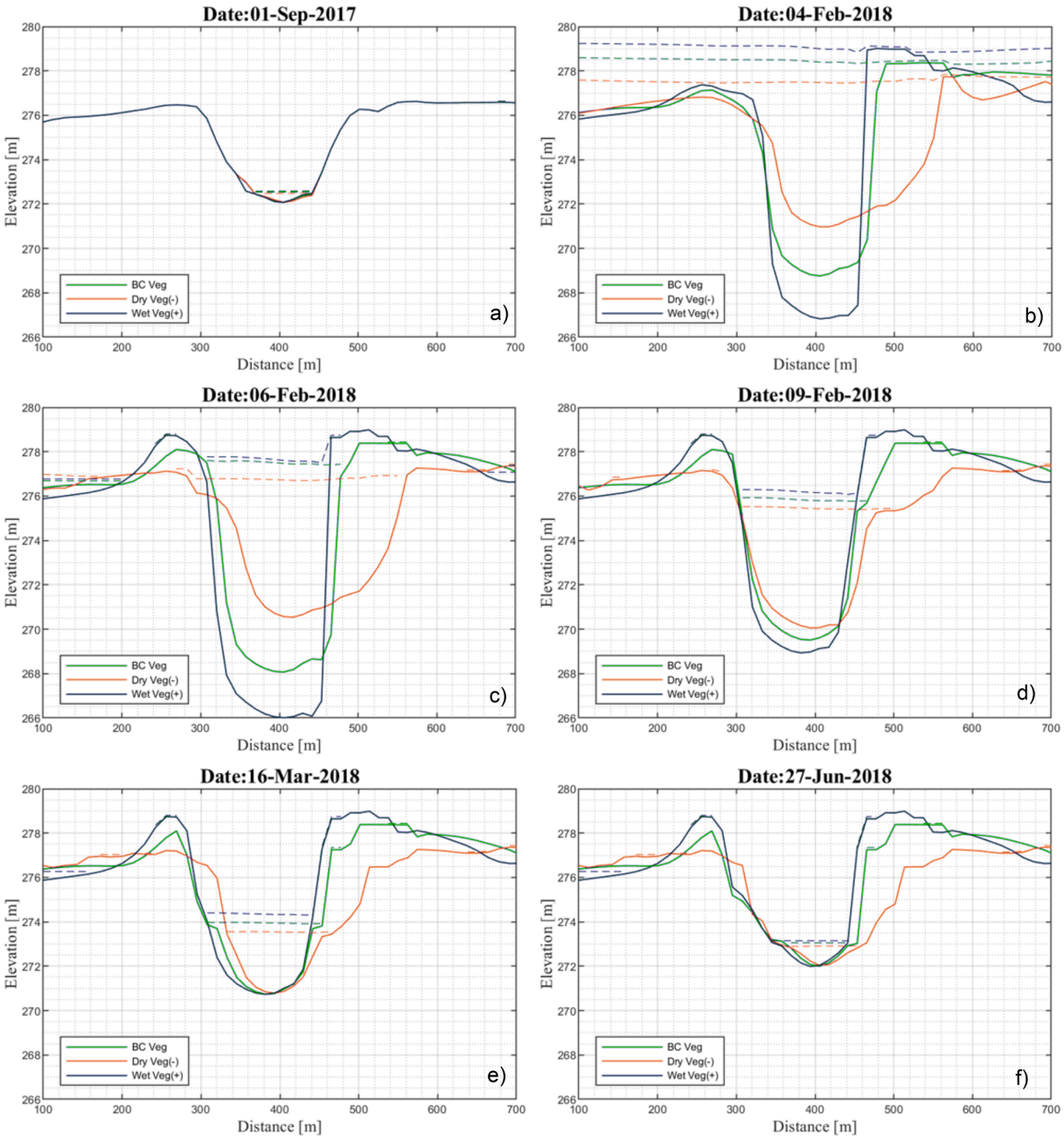

Fig. 8. Simulated bed level and water level profiles of Cross-Section A (Fig. 3) for the three different climates at different flow conditions. Water levels are indicated by dotted lines. Red: dry climate. Blue: present climate (Base Case). Blue: wet climate. (For interpretation of the references to colour in this figure legend, the reader is referred to the web version of this article.)

adaptation of the cross-sections of the Pilcomayo River (Fig. 2), well reproduced by the model (Fig. 5), allows relating the computed cross-section profiles to the discharge of the day. Almost no differences between climate scenarios can be observed at the start of the simulations when the flow is very low for all the three scenarios (e.g., on 1 September 2017 in Fig. 4). The quick morphological adaptations that occur during the flood season (January to March 2018) result in a systematically wider channel for the drier climate and in a systematically narrower channel for the wetter climate scenario. The three climate scenarios present a similar channel depth at low flows. However, the depth is substantially larger with the wetter climate scenario at the highest discharges, which is due to the higher flow rates and the denser vegetation which appears to successfully limit bank erosion. The result of the wet climate scenario is thus a higher transient channel excavation of 20 % respect to the current scenario (Fig. 8c). At the end of the wet season (Fig. 8f), when the flow is low again, the wet areas are similar for all the three considered climates. Sediment deposition, occurring during the falling limb of the flood waves, results in a similar bed level rise for all the three climates, since more sediment is transported and thus deposited with the wetter climate. Instead, the width is maintained and our results indicate that the bankfull width can be expected to increase by 35–45 % in 2100, due to the forecasted climate change (Fig. 8b-f).

Fig. 9 shows the yearly sand transport rates of the river for all the considered scenarios. An increase in sediment transport rates can be expected if the climate becomes wetter (+46.1 %); a decrease if the climate becomes drier (-39.1 %). Fig. 9 allows also detecting the effects of changes in floodplain vegetation. In combination with the present discharge hydrograph (green bars), either a higher or a lower vegetation

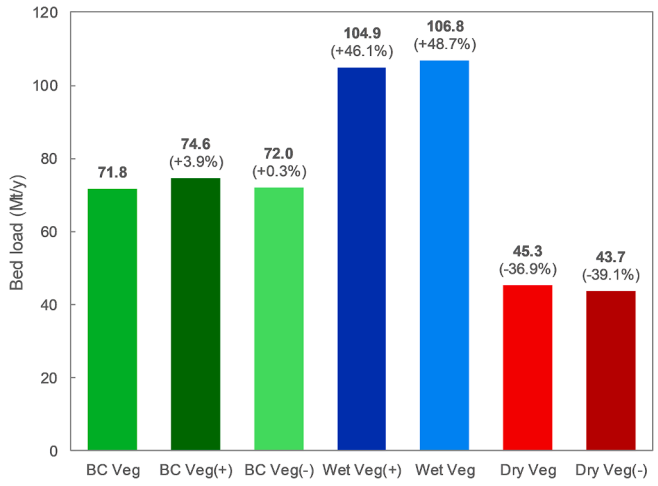

Fig. 9. Cumulative transported bed material load (sand), excluding wash load. Between parentheses: changes in percentage compared to the present climate (BC Veg).

mass would increase the yearly sediment transport rates. A denser vegetation, Veg(+), would increase the sediment transport capacity of the flow by enhancing its concentration, and velocity, in the main channel (+3.9 %). A lower floodplain vegetation mass, Veg(-), would increase the sediment input through a slight increase in bank erosion (+0.3 %). A similar effect of vegetation is found in combination with the drier hydrograph (red bars). Instead, a larger vegetation mass, Veg(+), would, but only slightly, decrease the yearly sediment transport rate in combination with the wetter hydrograph (blue bars). This is mainly due bank erosion zeroing. Finally, it is important to consider that these results exclude wash load. Including the finest part of the sediment transported by the flow would not affect the configuration of the main river channel, but would result in higher floodplain sedimentation rates, with deposition occurring further away from the main channel margin than sand.

Fig. 10 shows the water coverage in the study area with the present discharge hydrograph, but without floodplain vegetation on February 4th 2018 (peak flow of 3,934 m^3/s). On that day, being the discharge above bankfull, it is possible to detect the presence of channels excavated through the floodplains. In this case, the river presents multiple channel excavation and main channel shift, resulting in a braided system with substantial straightening: the present channel sinuosity is 1.3, calculated as average sinuosity in the period 1972–2017 (Table 1), while the predicted sinuosity without floodplain vegetation (under the "BC noVeg" scenario) is 1.1 (Fig. 10). Considering that the downstream boundary conditions (water levels) and the upstream boundary conditions (2D flow distribution) are the same, river straightening means also steepening of the longitudinal water level profile. And indeed, the longitudinal slope increases from 0,038 % (present situation, Table 1) to 0.044 % (Fig. 10).

6. Discussion

The model covers one hydrological year to shows how the river cross-section evolves with different climatic and vegetation settings. Since the morphodynamic response of rivers is complex and depends on sequences of floods and dry periods, we needed a real hydrograph as basis to construct the drier and wetter scenarios. In fact, we could not reproduce the morphodynamic river response with annual or seasonal mean streamflows. Additionally, the choice of covering one year is justified by the intrinsic morphodynamics of the Pilcomayo River, our case study. This river has such a strong dynamic that the cross-section drastically changes every day as a response to the discharge variation. For this reason and after having well reproduced this behavior with the model and analyzed its morphodynamics (Chapter 5), we decided that we can link the cross-section that is measured in one day to the discharge. Ultimately, this work does not want to forecast the Pilcomayo River morphology due to global change, but, more in general, to disentangle the river response to plausible dryer and wetter scenarios. A specific further study on how the Pilcomayo will evolve in the future due to climate change would be certainly an important contribution.

In our model, sediment input is computed as a function of inflow characteristics using the sediment transport formula of van Rijn (1984) which includes suspended load and is particularly appropriate for fine sand. As all transport capacity formulas, van Rijn's does not include wash load, i.e. the transport of very fine material, silt and clay, which is supply-limited rather than capacity-limited. Thus, the decrease in discharge characterizing the dry climate also results in reduced sediment input to the study area, whereas for the wetter climate our model predicts larger sediment inputs. Wash load supply is mainly related to soil erosion in the river catchment. In this study, we do not consider the effects of changing climate on sediment production (Pitlick et al., 2012; Verhaar et al., 2010). The reduction of vegetation cover due to a drier climate is expected to result in increased soil erodibility in the river catchment and larger sediment inputs to the river. The transport of sand, which is capacity-limited, is expected to decrease if the discharges decrease (Fig. 9). However, dry climates often present extreme discharge variations due to rainfall concentration in brief periods, so it is not clear whether higher, but shorter, discharge peaks would actually increase or decrease the total bed load in the river.

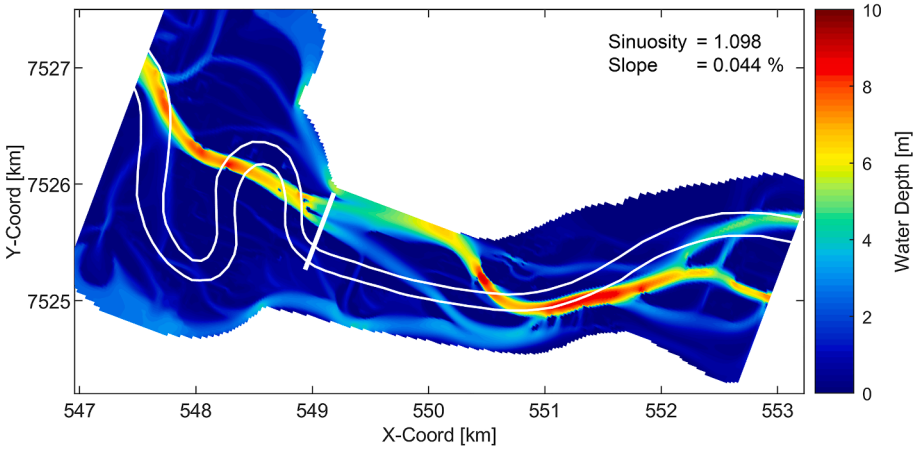

Fig. 10. Simulated water depth over the entire model domain on 04 Feb 2018: present discharge hydrograph without floodplain vegetation ("BC noVeg" scenario). The thick white line depicts the plane delineation of the current channel; the straight white line across the channel indicates the location of Cross-Section A (Fig. 10).

As a result of an increase in sediment load, we can expect enhanced bed aggradation to occur where the slope of the river decreases, further enhancing the tendency towards a braided style at these locations (Germanoski and Schumm, 1993). A wetter climate would have opposite effects, i.e. reduction of sediment production, enhancing a meandering style (Gurnell, 2012).

The effects of vegetation on hydraulic resistance, sediment transport and bed erosion are included in the model in a static way by assuming a certain distribution of plants with constant characteristics (height, density, representative diameter) on the floodplain, depending on scenario. However, vegetation processes (colonization, growth, decay) are known to interact with the river dynamics (Caponi et al., 2020; van Oorschot et al., 2016) and are affected by climate (Liu and Lei, 2015; Roerink et al., 2003). Lack of data and the choice to concentrate the analysis in one hydrological year do not allow including vegetation dynamics. This means that our work does not represent the transition period, i.e. when the river channel evolves until the characteristics of the floodplain vegetation reach the configuration expected in the future climate.

By including the effects of vegetation on water flow and sediment transport, the model indirectly reproduces also part of the protecting effects of plants on river banks. Due to the higher roughness caused by riparian vegetation, the main flow is deflected towards the centre of the channel, and the near-bank flow velocity as well as the near-bank bed shear stress are reduced. This decreases erosion of the river bed near the bank, which our model partially converts in bank erosion (van Der Wegen and Roelvink, 2008), and enhances levee formation (Crosato and Saleh, 2011). The model ignores bank strengthening by roots and bank reinforcement by slump blocks that armour cut banks. In addition, the model does not account for vegetation dynamics, in terms of colonization, growth and decay of plants. This becomes important in river systems where plants have the possibility to colonize emerging bars and banks during low flows and have the time to grow strong enough to resist the next flood (Serlet et al., 2018). In rivers where plant dynamics plays a role, this is found to enhance bank accretion and opposite bank erosion, which results in increased river meandering (Vargas-Luna et al., 2019b).

As previously described, measured data on plant colonization, growth, temporal changes in plant density, etc. are lacking. The only vegetation data available for this study is the type of vegetation that is dominant in the area whereas we derived historical floodplain vegetation cover distribution from satellite images. Vegetation dynamics depends not only on plant species, but also on climate, soil type and moisture, which means that we could derive this information from studies carried out elsewhere. Along the Pilcomayo, vegetation is mainly present on the floodplain and rarely on bars, a clear sign that vegetation processes are governed by the river dynamics and do not play a relevant role in the cross-sectional dynamics of the river. Vargas-Luna, Duró, et al. (2019b) showed that colonization of emerging bars by vegetation increases opposite bank erosion, but does not affect channel width and depth, focus of this research. Not considering vegetation dynamics could be a shortcoming in the generalization of the results for sand-bed rivers in different climatic settings. Moreover, considering that the interaction river-vegetation is affected by scale (Gurnell, 2014), we conclude that our study case and the results herein presented are strictly representative of rivers having size compared to Pilcomayo's, located in similar climatic settings and having similar hydro-morphological conditions. In any case, our results indicate the right trends of river morphological variations under moderate climate change in general, and that our results can be used as a guidance to include climate change effects in forecasting the long term evolution of rivers. The results of this study provide also a reference tool to analyse past changes of river environments assuming no human influence. The results provide also an insight to predict the effects of combinations of interventions, for instance regarding floodplain vegetation management (e.g.: González et al., 2017) and alterations of the river discharge on the width and depth of the main river channel (e.g.: Su et al., 2021).

Table 3
Main channel sinuosity and slope for the studied scenarios.

Scenario	Sinuosity	Slope
Present (2017, Fig. 3)	1.603	0.030
Dry veg(-)	1.477	0.033
Wet veg(+)	1.493	0.032
BC noVeg (Fig. 10)	1.098	0.044

A recent study (Chen et al., 2019) shows that the hydrological regime leaves an imprint on the longitudinal profile of rivers. In particular, based on NASA data sets and numerical modelling, Chen et al. (2019) show that drier climates (aridity) reduce the river sinuosity and produce steeper longitudinal slopes. Our results show that the absence of floodplain vegetation increases the longitudinal slope of the river through channel straightening as a result of river braiding (Fig. 10). Overall, a light flow straightening is also obtained for the moderately drier climate (see Table 3). Thus our results appear to support Chen et al.'s observations.

The central region of the study area has remained straight for at least the period covered by our study (1972–2018). We do not have data explaining this, which might be due to either artificial or natural (vegetation) bank reinforcement or to the characteristics of the bank material in that region. To explain this, we recommend carrying out some field investigations focusing on the characterization of the river banks.

7. Conclusions

This numerical study analyses the adaptation to climate of sand-bed rivers, considering the Pilcomayo as an example. For the climate scenarios, we considered the 2100 projections of the Intergovernmental Panel on Climate Change (IPCC) Special Report on Emission Scenario A1B, hereafter named as the SRES A1B scenario (Stocker et al., 2013). Our model reproduces historical cross-sectional changes that follow the measured ones, which gives confidence in our results. We then used the model to assess the response of the main river channel to climate change, considering the forecast for the year 2100, as well as its opposite, the river climate being described by a combination of hydrological regime and floodplain vegetation characteristics.

The main finding of this investigation results from the analysis of the either combined or separate effects of alterations in discharge regime and floodplain vegetation, both resulting from climate change. These alterations interact with each-other and affect the river morphology in a non-linear way, complicating the analysis of their single roles in the process of climate adaptation. Our results show that for moderate climate changes vegetation governs the river channel width whereas discharge, in presence of floodplain vegetation, mainly affects the main channel depth and the levee formation. Previous works not considering the role of riparian vegetation found a much stronger effect of discharge alteration on channel width (e.g.: Vargas-Luna et al., 2019b). The difference is mainly due to having now considered the effects of plants on river banks, which is obtained in our model only partially, since the strengthening effects of roots and the mechanical reinforcement of slump blocks that shelter failed banks and limit further erosion are not considered. Due to this, we can expect plants to have an even stronger role in governing the river width than our results are able to demonstrate.

Previous works have shown that floodplain vegetation growth lead to important changes of the river morphology which even result in a different fluvial style, for instance from braiding to meandering (e.g.: Crosato and Saleh, 2011; Gurnell, 2014; Tal and Paola, 2010; Villada Arroyave and Crosato, 2010). This is confirmed also by the results of our study, showing that without vegetation the Pilcomayo River would be braided.

Summarising, we find that for sand-bed rivers in temperate climates:

- A moderately dryer climate, characterized by reduced water flow and scarcer floodplain vegetation, will result in a shallower and wider water course with floodplains and banks that are more prone to erosion. The projected change for the Pilcomayo River in 2100 is a consistent bankfull width increase by 35–45 % respect to the current scenario.
- A moderately wetter climate, characterized by increased water flow and denser floodplain vegetation, during floods will produce a transient deeper channel by 20 % respect to the current scenario, whereas channel widening will be limited by vegetation offering a more effective protection to cut banks.

8. Research data

The National Hydrological Network of Argentina has records for daily discharge, water level and cross-sectional profile at the station of Misión La Paz (in front of Pozo Hondo, 22°22′38″S, 62°31′24″W) from 1960 to 2018. The time series of discharges and water levels were downloaded from http://bdhi.hidricosargentina.gob.ar/. The time series of the cross-section was downloaded from www.pilcomayo.net, the webpage of the Tri-national Committee for the Development of the Pilcomayo River basin. Sediment data, including sediment characteristics, are also available from several documents at www.pilcomayo.net. The models are freely downloadable from the website of NCR (Netherlands Centre of River studies: https://ncr-web.org/).

CRediT authorship contribution statement

A. Crosato: Conceptualization, Methodology, Validation, Resources, Formal analysis, Writing – original draft, Writing – review & editing, Supervision, Project administration. **A. Grissetti-Vázquez:** Methodology, Software, Validation, Formal analysis, Investigation, Data curation, Writing – original draft, Visualization. **F. Bregoli:** Conceptualization, Validation, Formal analysis, Writing – original draft, Writing – review & editing, Visualization, Supervision. **M.J. Franca:** Writing – review & editing, Supervision, Project administration.

Declaration of Competing Interest

The authors declare that they have no known competing financial interests or personal relationships that could have appeared to influence the work reported in this paper.

Data availability

Data will be made available on request.

Acknowledgments

Alberto Grissetti carried out this research with funds from the World Meteorological Organization Fellowship Programme. Francesco Bregoli received funding from the EC Marie Curie Individual Fellowship, H2020 Priority Excellent Science [grant number 606838]. The authors wish to thank Dr. Sergio Capapé (Jacobs UK, formerly at Universitat Politècnica de Catalunya) for his important suggestions, Dr. Paolo Paron (IHE Delft) and Dr. Alessandro Ielpi (Laurentian University) for reviewing an early version of the manuscript, and to the National Committee of the Pilcomayo River in Paraguay for providing access to their database.

References

Anadón, J.D., Sala, O.E., Maestre, F.T., 2014. Climate change will increase savannas at the expense of forests and treeless vegetation in tropical and subtropical Americas. J. Ecol. 102, 1363–1373. https://doi.org/10.1111/1365-2745.12325.

Arboleda, A.M., Crosato, A., Middelkoop, H., 2010. Reconstructing the early 19th-century Waal River by means of a 2D physics-based numerical model. Hydrol. Process. 24 https://doi.org/10.1002/hyp.7804.

Baar, A.W., Boechat Albernaz, M., van Dijk, W.M., Kleinhans, M.G., 2019. Critical dependence of morphodynamic models of fluvial and tidal systems on empirical downslope sediment transport. Nat. Commun. Doi: 10.1038/s41467-019-12753-x.

Baker, W.L., 1995. Longterm response of disturbance landscapes to human intervention and global change. Landsc. Ecol. 10, 143–159. https://doi.org/10.1007/BF00133028.

Baldissone, C., Gyssels, P., Spalletti, P., Brea D, D., Testa Tacchino, A.J.S., Hillman, G., Rodríguez, A., Zambón, H., 2013. Modelación Hidrodinámica Bidimensional de las Intervenciones para la Distribución de las Aguas del Río Pilcomayo entre Argentina y Paraguay, in: XXIV Congreso Nacional Del Agua. INA-CIRSA Córdoba, Argentina, San Juan.

Baptist, M.J., de Jong, J.F., 2005. Modelling the influence of vegetation on the morphology of the Allier, France, in: COST 626. Silkeborg, Denmark.

Baptist, M.J., Babovic, V., Uthurburu, J.R., Keijzer, M., Uittenbogaard, R.E., Mynett, A., Verwey, A., 2007. On inducing equations for vegetation resistance. J. Hydraul. Res. https://doi.org/10.1080/00221686.2007.9521778.

Boothroyd, R.J., Nones, M., Guerrero, M., 2021. Deriving Planform Morphology and Vegetation Coverage From Remote Sensing to Support River Management Applications. Front. Environ. Sci. 9.

Borrelli, P., Robinson, D.A., Fleischer, L.R., Lugato, E., Ballabio, C., Alewell, C., Meusburger, K., Modugno, S., Schütt, B., Ferro, V., Bagarello, V., Oost, K.V., Montanarella, L., Panagos, P., 2017. An assessment of the global impact of 21st century land use change on soil erosion. Nat. Commun. 8 https://doi.org/10.1038/s41467-017-02142-7.

Brea, J.D., Spalletti, P., Irigoyen, M.A., Hillman, G., Gyssels, P., Baldissone, C.M., 2014. Modelación Matemática del Río Pilcomayo en la zona de la Embocadura.

Cai, W., Borlace, S., Lengaigne, M., Van Rensch, P., Collins, M., Vecchi, G., Timmermann, A., Santoso, A., Mcphaden, M.J., Wu, L., England, M.H., Wang, G., Guilyardi, E., Jin, F.F., 2014. Increasing frequency of extreme El Niño events due to greenhouse warming. Nat. Clim. Chang. 4, 111–116. https://doi.org/10.1038/nclimate2100.

Capape, S., Martin-Vide, J.P., 2015. Evidence of transient scour and fill, in: E-Proceedings of the 36th IAHR World Congress. The Hague.

Caponi, F., Vetsch, D.F., Siviglia, A., 2020. A model study of the combined effect of above and below ground plant traits on the ecomorphodynamics of gravel bars. Sci. Rep. 10, 17062. https://doi.org/10.1038/s41598-020-74106-9.

Chen, S.-A., Michaelides, K., Grieve, S.W.D., Singer, M.B., 2019. Aridity is expressed in river topography globally. Nature. https://doi.org/10.1038/s41586-019-1558-8.

Church, M., 2006. Bed material transport and the morphology of alluvial river channels. Annu. Rev. Earth Planet. Sci. 34, 325–354. https://doi.org/10.1146/annurev.earth.33.092203.122721.

Coulthard, T.J., 2005. Effects of vegetation on braided stream pattern and dynamics. Water Resour. Res. 41. https://doi.org/10.1029/2004WR003201.

Crosato, A., Mosselman, E., 2020. An Integrated Review of River Bars for Engineering, Management and Transdisciplinary Research. Water. Doi: 10.3390/w12020596.

Crosato, A., Mosselman, E., 2009. Simple physics-based predictor for the number of river bars and the transition between meandering and braiding. Water Resour. Res. 45 https://doi.org/10.1029/2008WR007242.

Crosato, A., Saleh, M.S., 2011. Numerical study on the effects of floodplain vegetation on river planform style. Earth Surf. Process. Landforms 36, 711–720. https://doi.org/10.1002/esp.2088.

Dale, V.H., Joyce, L.A., McNulty, S., Neilson, R.P., Ayres, M.P., Flannigan, M.D., Hanson, P.J., Irland, L.C., Lugo, A.E., Peterson, C.J., 2001. Climate change and forest disturbances: climate change can affect forests by altering the frequency, intensity, duration, and timing of fire, drought, introduced species, insect and pathogen outbreaks, hurricanes, windstorms, ice storms, or landslides. Bioscience 51, 723–734.

Deltares, 2019. Delft3D-FLOW, Simulation of multi-dimensional hydrodynamic flows and transport phenomena, including sediments, Version, 3. ed. Delft, The Netherlands.

Engelund, F., Hansen, E., 1967. A monograph on sediment transport in alluvial streams, Denmark Tech. Univ. TEKNISKFORLAG Skelbrekgade 4 Copenhagen V, Denmark.

Exner, F.M., 1920. Zur physik der dunen. Akad. Wiss. Wien Math 129 (2a), 165–204.

Fernández, R., Garcia, M.H., 2017. Input-variable sensitivity assessment for sediment transport relations. Water Resour. Res. 53, 8105–8119. https://doi.org/10.1002/2016WR020249.

Germanoski, D., Schumm, S.A., 1993. Changes in braided river morphology resulting from aggradation and degradation. J. Geol. https://doi.org/10.1086/648239.

Gibling, M.R., Davies, N.S., 2012. Palaeozoic landscapes shaped by plant evolution. Nat. Geosci. https://doi.org/10.1038/ngeo1376.

González, E., Masip, A., Tabacchi, E., Poulin, M., 2017. Strategies to restore floodplain vegetation after abandonment of human activities. Restor. Ecol. 25, 82–91. https://doi.org/10.1111/rec.12400.

Grams, P.E., Schmidt, J.C., 2005. Equilibrium or indeterminate? Where sediment budgets fail: Sediment mass balance and adjustment of channel form, Green River downstream from Flaming Gorge Dam, Utah and Colorado. Geomorphology 71, 156–181. https://doi.org/10.1016/j.geomorph.2004.10.012.

Gurnell, A., 2012. Fluvial geomorphology: Wood and river landscapes. Nat. Geosci. 5, 93–94. https://doi.org/10.1038/ngeo1382.

Gurnell, A., 2014. Plants as river system engineers. Earth Surf. Process. Landforms 39, 4–25. https://doi.org/10.1002/esp.3397.

Halcrow & Serman Associados, 2006. Línea Base Ambiental y Socioeconómica de la cuenca del Río Pilcomayo. Tarija, Bolivia: Proyecto de Gestión Integrada y Plan Maestro de la Cuenca del Río Pilcomayo.
Harrison, S., Mighall, T., Stainforth, D.A., Allen, P., Macklin, M., Anderson, E., Knight, J., Mauquoy, D., Passmore, D., Rea, B., Spagnolo, M., Shannon, S., 2019. Uncertainty in geomorphological responses to climate change. Clim. Change 156, 69–86. https://doi.org/10.1007/s10584-019-02520-8.
Hupp, C.R., Simon, A., 1991. Bank accretion and the development of vegetated depositional surfaces along modified alluvial channels. Geomorphology 4, 111–124. https://doi.org/10.1016/0169-555X(91)90023-4.
Ielpi, A., Lapôtre, M.G.A., 2019. Biotic forcing militates against river meandering in the modern Bonneville Basin of Utah. Sedimentology 66, 1896–1929. https://doi.org/10.1111/sed.12562.
Koch, F.G., Flokstra, C., 1980. Bed Level Computations for Curved Alluvial Channels, in: 19th IAHR Congress, New Delhi, India, February 1981. Waterloopkundig Laboratorium, New Delhi, India.
Kondolf, G.M., 1997. Hungry water: Effects of dams and gravel mining on river channels. Environ. Manage. https://doi.org/10.1007/s002679900048.
Lane, S.N., Tayefi, V., Reid, S.C., Yu, D., Hardy, R.J., 2007. Interactions between sediment delivery, channel change, climate change and flood risk in a temperate upland environment. Earth Surf. Process. Landforms 32, 429–446. https://doi.org/10.1002/esp.1404.
Leopold, L.B., Wolman, M.G., 1957. River channel patterns: Braided, meandering, and straight, Professional Paper. Washington, D.C. Doi: 10.3133/pp282B.
Lesser, G.R., Roelvink, J.A., van Kester, J.A.T.M., Stelling, G.S., 2004. Development and validation of a three-dimensional morphological model. Coast. Eng. https://doi.org/10.1016/j.coastaleng.2004.07.014.
Lightbody, A.F., Kui, L., Stella, J.C., Skorko, K.W., Bywater-Reyes, S., Wilcox, A.C., 2019. Riparian Vegetation and Sediment Supply Regulate the Morphodynamic Response of an Experimental Stream to Floods. Front. Environ. Sci. 7.
Liu, Y., Lei, H., 2015. Responses of Natural Vegetation Dynamics to Climate Drivers in China from 1982 to 2011. Remote Sens. 7, 10243–10268. https://doi.org/10.3390/rs70810243.
Martín-Vide, J.P., Amarilla, M., Zárate, F.J., 2014. Collapse of the Pilcomayo River. Geomorphology. https://doi.org/10.1016/j.geomorph.2012.12.007.
Martín-Vide, J.P., Capape, S., Ferrer-Boix, C., 2019. Transient scour and fill. The case of the Pilcomayo River. J. Hydrol. 576, 356–369. https://doi.org/10.1016/j.jhydrol.2019.06.041.
Masson-Delmotte, V., Zhai, P., Pörtner, H.-O., Roberts, D., Skea, J., Shukla, P.R., Pirani, A., Moufouma-Okia, W., Péan, C., Pidcock, R., Connors, S., Matthews, J.B.R., Chen, Y., Zhou, X., Gomis, M.I., Lonnoy, E., Maycock, T., Tignor, M., Waterfield, T., 2018. Global warming of 1.5°C An IPCC Special Report, Report of the Intergovernmental Panel on Climate Change.
Micheli, E.R., Kirchner, J.W., 2002. Effects of wet meadow riparian vegetation on streambank erosion. 2. Measurements of vegetated bank strength and consequences for failure mechanics. Earth Surf. Process. Landforms 27, 687–697. https://doi.org/10.1002/esp.340.
Montroull, N.B., Saurral, R.I., Camilloni, I.A., 2018. Hydrological impacts in La Plata basin under 1.5, 2 and 3 °C global warming above the pre-industrial level. Int. J. Climatol. 38, 3355–3368. https://doi.org/10.1002/joc.5505.
Moriasi, D.N., Gitau, M.W., Pai, N., Daggupati, P., 2015. Hydrologic and water quality models: Performance measures and evaluation criteria. Trans. ASABE. Doi: 10.13031/trans.58.10715.
Nardi, L., Campo, L., Rinaldi, M., 2013. Quantification of riverbank erosion and application in risk analysis. Nat. Hazards 69, 869–887. https://doi.org/10.1007/s11069-013-0741-8.
Nepf, H.M., 2012. Flow and Transport in Regions with Aquatic Vegetation. Annu. Rev. Fluid Mech. https://doi.org/10.1146/annurev-fluid-120710-101048.
O'Hare, M.T., Mountford, J.O., Maroto, J., Gunn, I.D.M., 2016. Plant Traits Relevant To Fluvial Geomorphology and Hydrological Interactions. River Res. Appl. 32, 179–189. https://doi.org/10.1002/rra.2940.
Pasquale, N., Perona, P., Francis, R., Burlando, P., 2014. Above-ground and below-ground Salix dynamics in response to river processes. Hydrol. Process. 28, 5189–5203. https://doi.org/10.1002/hyp.9993.
Peel, M.C., Finlayson, B.L., McMahon, T.A., 2007. Updated world map of the Köppen-Geiger climate classification. Hydrol. Earth Syst. Sci. https://doi.org/10.5194/hess-11-1633-2007.
Perona, P., Molnar, P., Crouzy, B., Perucca, E., Jiang, Z., McLelland, S., Wüthrich, D., Edmaier, K., Francis, R., Camporeale, C., Gurnell, A., 2012. Biomass selection by floods and related timescales: Part 1. Experimental observations. Adv. Water Resour. 39, 85–96. https://doi.org/10.1016/j.advwatres.2011.09.016.
Pitlick, J., Mueller, E.R., Segura, C., 2012. Differences in Sediment Supply to Braided and Single-Thread River Channels: What Do the Data Tell Us?, in: Gravel-Bed Rivers: Processes, Tools, Environments. Doi: 10.1002/9781119952497.ch35.
Pool, M.A., Van Duijne, J.D.G., 1996. Informe final de la tercera misión de asistencia técnica enviada por la comisión de la UE a la zona del Pilcomayo. Proyecto de gestión Integrada y Plan Maestro de la Cuenca del Rio Pilcomayo. Paraguay-Argentina.
Roerink, G.J., Menenti, M., Soepboer, W., Su, Z., 2003. Assessment of climate impact on vegetation dynamics by using remote sensing. Phys. Chem. Earth, Parts A/B/C 28, 103–109. https://doi.org/10.1016/S1474-7065(03)00011-1.
Rominger, J.T., Lightbody, A.F., Nepf, H.M., 2010. Effects of Added Vegetation on Sand Bar Stability and Stream Hydrodynamics. J. Hydraul. Eng. 136, 994–1002. https://doi.org/10.1061/(asce)hy.1943-7900.0000215.
Sabater, S., Bregoli, F., Acuña, V., Barceló, D., Elosegi, A., Ginebreda, A., Marcé, R., Muñoz, I., Sabater-Liesa, L., Ferreira, V., 2018. Effects of human-driven water stress on river ecosystems: a meta-analysis. Sci. Rep. 8, 11462. https://doi.org/10.1038/s41598-018-29807-7.
Sarker, M.H., Thorne, C.R., Aktar, M.N., Ferdous, M.R., 2014. Morpho-dynamics of the Brahmaputra-Jamuna River, Bangladesh. Geomorphology 215, 45–59. https://doi.org/10.1016/j.geomorph.2013.07.025.
Seneviratne, S.I., Lüthi, D., Litschi, M., Schär, C., 2006. Land-atmosphere coupling and climate change in Europe. Nature 443, 205–209. https://doi.org/10.1038/nature05095.
Serlet, A.J., Gurnell, A.M., Zolezzi, G., Wharton, G., Belleudy, P., Jourdain, C., 2018. Biomorphodynamics of alternate bars in a channelized, regulated river: An integrated historical and modelling analysis. Earth Surf. Process. Landforms 43, 1739–1756. https://doi.org/10.1002/esp.4349.
Singh, U., Crosato, A., Giri, S., Hicks, M., 2017. Sediment heterogeneity and mobility in the morphodynamic modelling of gravel-bed braided rivers. Adv. Water Resour. 104, 127–144. https://doi.org/10.1016/j.advwatres.2017.02.005.
Siviglia, A., Crosato, A., 2016. Numerical modelling of river morphodynamics: Latest developments and remaining challenges. Adv. Water Resour. https://doi.org/10.1016/j.advwatres.2016.01.005.
Solari, L., Van Oorschot, M., Belletti, B., Hendriks, D., Rinaldi, M., Vargas-Luna, A., 2016. Advances on Modelling Riparian Vegetation-Hydromorphology Interactions. River Res. Appl. 32, 164–178. https://doi.org/10.1002/rra.2910.
Sperna Weiland, F.C., Van Beek, L.P.H., Kwadijk, J.C.J., Bierkens, M.F.P., 2012. Global patterns of change in discharge regimes for 2100. Hydrol. Earth Syst. Sci. 16, 1047–1062. https://doi.org/10.5194/hess-16-1047-2012.
Stocker, T.F., Qin, D., Plattner, G.K., Tignor, M.M.B., Allen, S.K., Boschung, J., Nauels, A., Xia, Y., Bex, V., Midgley, P.M., 2013. Climate change 2013 the physical science basis: Working Group I contribution to the fifth assessment report of the intergovernmental panel on climate change, Climate Change 2013 the Physical Science Basis: Working Group I Contribution to the Fifth Assessment Report of the Intergovernmental Panel on Climate Change. https://doi.org/10.1017/CBO9781107415324.
Struiksma, N., Olesen, K.W., Flokstra, C., De Vriend, H.J., 1985. Bed deformation in curved alluvial channels. J. Hydraul. Res. 23, 57–79. https://doi.org/10.1080/00221688509499377.
Su, T., Huang, H.Q., Carling, P.A., Yu, G., Nanson, G.C., 2021. Channel-Form Adjustment of an Alluvial River Under Hydrodynamic and Eco-Geomorphologic Controls: Insights From Applying Equilibrium Theory Governing Alluvial Channel Flow. Water Resour. Res. 57, e2020WR029174. Doi: 10.1029/2020WR029174.
Tal, M., Paola, C., 2010. Effects of vegetation on channel morphodynamics: Results and insights from laboratory experiments. Earth Surf. Process. Landforms 35, 1014–1028. https://doi.org/10.1002/esp.1908.
Talmon, A.M., Struiksma, N., Van Mierlo, M.C.L.M., 1995. Laboratory measurements of the direction of sediment transport on transverse alluvial-bed slopes. J. Hydraul. Res. 33, 495–517. https://doi.org/10.1080/00221689509498657.
Testa Tacchino, A.J.S., 2015. Caracterización de desbordes del río Pilcomayo entre Villamontes y Misión La Paz. Universidad Nacional de Córdoba, Argentina.
Thorne, C.R., 1982. Processes and mechanisms of river bank erosion., in: Gravel-Bed Rivers. Wiley: Chichester, pp. 227–271.
Trenberth, K.E., 2011. Changes in precipitation with climate change. Clim. Res. 47, 123–138. https://doi.org/10.3354/cr00953.
Van Beek, L.P.H., Bierkens, M.F.P., 2009. The Global Hydrological Model PCR-GLOBWB: Conceptualization. Parameterization and Verification, Utrecht.
van Der Wegen, M., Roelvink, J.A., 2008. Long-term morphodynamic evolution of a tidal embayment using a two-dimensional, process-based model. J. Geophys. Res. Ocean. https://doi.org/10.1029/2006JC003983.
van Oorschot, M., Kleinhans, M., Geerling, G., Middelkoop, H., 2016. Distinct patterns of interaction between vegetation and morphodynamics. Earth Surf. Process. Landforms 41, 791–808. https://doi.org/10.1002/esp.3864.
van Oorschot, M., Kleinhans, M., Buijse, T., Geerling, G., Middelkoop, H., 2018. Combined effects of climate change and dam construction on riverine ecosystems. Ecol. Eng. 120, 329–344. https://doi.org/10.1016/J.ECOLENG.2018.05.037.
van Rijn, L.C., 1984. Sediment transport, part II: Suspended load transport. J. Hydraul. Eng. https://doi.org/10.1061/(ASCE)0733-9429(1984)110:11(1613).
van Vuuren, D.P., Edmonds, J., Kainuma, M., Riahi, K., Thomson, A., Hibbard, K., Hurtt, G.C., Kram, T., Krey, V., Lamarque, J.-F., Masui, T., Meinshausen, M., Nakicenovic, N., Smith, S.J., Rose, S.K., 2011. The representative concentration pathways: an overview. Clim. Change 109, 5. https://doi.org/10.1007/s10584-011-0148-z.
Vargas-Luna, A., Crosato, A., Calvani, G., Uijttewaal, W.S.J., 2016. Representing plants as rigid cylinders in experiments and models. Adv. Water Resour. https://doi.org/10.1016/j.advwatres.2015.10.004.
Vargas-Luna, A., Crosato, A., Anders, N., Hoitink, A.J.F., Keesstra, S.D., Uijttewaal, W.S.J., 2018. Morphodynamic effects of riparian vegetation growth after stream restoration. Earth Surf. Process. Landforms. https://doi.org/10.1002/esp.4338.
Vargas-Luna, A., Crosato, A., Byishimo, P., Uijttewaal, W.S.J., 2019a. Impact of flow variability and sediment characteristics on channel width evolution in laboratory streams. J. Hydraul. Res. 57, 51–61. https://doi.org/10.1080/00221686.2018.1434836.
Vargas-Luna, A., Duró, G., Crosato, A., Uijttewaal, W., 2019b. Morphological Adaptation of River Channels to Vegetation Establishment: A Laboratory Study. J. Geophys. Res. Earth Surf. 124, 1981–1995. https://doi.org/10.1029/2018JF004878.
Verhaar, P.M., Biron, P.M., Ferguson, R.I., Hoey, T.B., 2010. Numerical modelling of climate change impacts on Saint-Lawrence River tributaries. Earth Surf. Process. Landforms. https://doi.org/10.1002/esp.1953.
Villada Arroyave, J.A., Crosato, A., 2010. Effects of river floodplain lowering and vegetation cover. Proc. ICE-Water Manag. 163 (9), 2010.

Wang, C., Zheng, S., Wang, P., Hou, J., 2015. Interactions between vegetation, water flow and sediment transport: A review. J. Hydrodyn. 27, 24–37. https://doi.org/10.1016/S1001-6058(15)60453-X.

Ward, P.D., Montgomery, D.R., Smith, R., 2000. Altered river morphology in South Africa related to the Permian-Triassic extinction. Science (80-.). 289, 1740–1743. https://doi.org/10.1126/science.289.5485.1740.

Wilby, R.L., Beven, K.J., Reynard, N.S., 2008. Climate change and fluvial flood risk in the UK: More of the same? Hydrol. Process. https://doi.org/10.1002/hyp.6847.

Wilkerson, G., Parker, G., 2011. Physical Basis for Quasi-Universal Relationships Describing Bankfull Hydraulic Geometry of Sand-Bed Rivers. J. Hydraul. Eng. 137, 739–753. https://doi.org/10.1061/(ASCE)HY.1943-7900.0000352.

Wohl, E., Bledsoe, B.P., Jacobson, R.B., Poff, N.L., Rathburn, S.L., Walters, D.M., Wilcox, A.C., 2015. The natural sediment regime in rivers: Broadening the foundation for ecosystem management. Bioscience. https://doi.org/10.1093/biosci/biv002.

Yang, D., Kanae, S., Oki, T., Koike, T., Musiake, K., 2003. Global potential soil erosion with reference to land use and climate changes. Hydrol. Process. 17, 2913–2928. https://doi.org/10.1002/hyp.1441.